21st Australasian Fluid Mechanics Conference
Adelaide, Australia
10-13 December 2018

# Anisotropy in the 3D multimode Richtmyer-Meshkov instability

**M. Groom**[1] **and B. Thornber**[1]

[1]School of Aerospace, Mechanical and Mechatronic Engineering
University of Sydney, New South Wales 2006, Australia

## Abstract

This paper examines anisotropy in the Richtmyer-Meshkov instability (RMI) for a given three-dimensional, narrowband, multimodal perturbation, and whether anisotropy persists at later times when the mixing layer is tending towards self-similar growth. In particular, the degree to which viscous dissipation and molecular diffusion affect anisotropy is investigated by comparing the results of a low Reynolds number direct numerical simulation (DNS) with a high Reynolds number large eddy simulation (LES) for the same initial condition and numerical framework, as well as a LES of a quarter-scale initial condition, implemented in the University of Sydney high-order finite-volume code FLAMENCO. Various measures of anisotropy are considered, including ratios of the components of domain integrated turbulent kinetic energy and enstrophy, ratios of directional Taylor-scale Reynolds numbers and Lumley's anisotropy tensor. The results from the standard LES case show that the flow field is persistently anisotropic in the shock-parallel direction at the latest time considered, while comparisons with the DNS results show that anisotropy is moderately increased at low Reynolds number although tending towards the high Reynolds number results at later times. For the quarter-scale LES it can be seen that at very late times the layer is relaxing towards isotropy although a significant amount of anisotropy remains at the latest time, indicating that any eventual return to isotropy occurs over a very long time scale.

## Introduction

The Richtmyer–Meshkov instability (RMI) occurs when a perturbed interface separating two materials is impulsively accelerated, typically by a shock wave [12, 8]. The instability evolves due to the misalignment of density and pressure gradients at the interface, referred to as the deposition of baroclinic vorticity. This deposition leads to a net growth of the interface and the development of secondary Kelvin-Helmholtz instabilities, which drive the transition to a turbulent mixing layer. Unlike the closely related Rayleigh–Taylor instability, RMI can be induced for both light-heavy and heavy-light configurations, and in both cases the initial growth of the interface is linear and can be described by analytically. However, as the perturbation amplitudes become large with respect to the wavelength the layer growth enters the nonlinear regime, whereby numerical simulation is required to calculate the subsequent evolution. For a comprehensive and up-to-date review of the literature on RMI, the reader is referred to Zhou [24, 25].

The understanding of mixing due to RMI is of great importance in areas such as inertial confinement fusion (ICF) [3], supernovae dynamics [2] and supersonic combustion [22]. In all of these applications, quantitative experimental data is difficult to obtain, therefore gaining an understanding of the underlying physics relies to a considerable extent upon the use of numerical simulation. Furthermore, given the broad range of scales involved in practical applications (such as those mentioned above), as well as the fact that often other physics must be considered such as radiation or chemical/nuclear reactions, it is currently necessary to model the effects of mixing and turbulence to some degree in order to maintain computational tractability. This motivates the use of high-fidelity simulation techniques such as large eddy simulation (LES) and direct numerical simulation (DNS) for fundamental problems with the purpose of increasing the understanding of turbulent mixing and guiding the development of Reynolds-Averaged Navier-Stokes (RANS) and other reduced-order modelling techniques.

Previous numerical studies of this instability have demonstrated the ability of large eddy simulation (LES) algorithms to predict mixing at late time due to turbulent stirring in the high Reynolds number limit, [23, 17, 7, 19], with good agreement shown in various integral measures such as width and mixedness across a number of different codes [15]. With regards to ICF, recent simulations have indicated that the capsule hot spot is very viscous due to the high temperatures involved, hence the assumption of turbulent conditions in the hot spot is likely incorrect as small-scale mixing should be viscously damped [21]. It is also possible that ablator material is spread through the hotspot via molecular diffusion [3], which motivates the use of numerical simulation techniques such as DNS in order to explore the effects of these molecular transport processes (i.e. Reynolds number effects) on the evolution of RMI as well as to gain a better understanding of transitional behaviour.

An area where there is less clear agreement between various numerical as well as experimental studies is on the level of anisotropy that persists after the passage of the shock wave, an important consideration for the development of models for these types of flows. Tritschler *et al.* [20] found that for low Reynolds number DNS of RMI at three different Mach numbers the decay rates of turbulent kinetic energy (TKE) and enstrophy, as well as probability density functions of the velocity and its longitudinal and transverse derivatives, are in good agreement with values for decaying isotropic turbulence [20]. However various high Reynolds number LES studies simulating RMI induced mixing layers to late time have shown that there is persistent anisotropy in the TKE components, with the component in the shock direction typically having 30-60% higher energy [17, 10, 15]. Similar observations have also been made experimentally [11].

Other studies have used different measures of isotropy, for example Lombardini *et al.* [7] considered an anisotropy measure of the velocity power spectra for a range of different Mach numbers and found that at late time there was substantial, although not complete, isotropisation particularly at higher wavenumbers [7]. The same study also used the ratio of Taylor-scale Reynolds numbers (which is based on both TKE and dissipation rate) as an anisotropy measure, and found that this ratio tended to a value of $\approx 1.5$ at late time for all Mach numbers considered. It is also likely that the level of anisotropy depends on initial conditions, as evidenced by gas curtain experiments [1] and studies that have looked at the effects of different RMS slopes of the initial interface such as [4], which quantified anisotropy using the diagonal components of Lumley's anisotropy tensor. Mohaghar *et al.* [9] also investigated anisotropy using this measure and found that significant anisotropy exists prior to reshock in both single-mode and multi-mode cases.

Given the differing results and conclusions with regards to anisotropy in RMI induced mixing, the focus of the present study is to compare four measures of anisotropy for the results of three numerical simulations; a high Reynolds number implicit LES (ILES) and a low Reynolds number DNS of the same initial condition, as well as an ILES of a scaled version of the initial condition so as to allow for a much later non-dimensional time to be simulated. The ILES results have been documented previously in [15] (although not for all of the quantities considered here), whilst the DNS results are entirely new.

#### Problem Description

The equations solved are the compressible multicomponent Navier-Stokes equations (Euler equations in the case of ILES), which govern the behaviour of mixtures of miscible gases [6]. All cases presented here use the ideal gas equation of state, with Newton's law of viscosity, Fourier's law of conductivity and Fick's law of diffusion used to model molecular transport in the DNS. Note that the enthalpy flux, which arises due to changes in internal energy due to mass diffusion, must also be included in the DNS in order to correctly calculate the temperature of the mixture.

The governing equations are solved using the University of Sydney code `Flamenco`, which employs a Godunov-type method of lines approach in a structured multiblock framework. Spatial reconstruction of the inviscid terms is performed using a fifth order MUSCL scheme [5], augmented by a modification to the reconstruction procedure to ensure the correct scaling of pressure and velocity and therefore reduced numerical dissipation at low Mach number [16]. The inviscid flux component is then calculated using the HLLC Riemann solver [18], while the viscous and diffusive terms present in the DNS are computed using second order central differences. Temporal integration is achieved via a second order TVD Runge–Kutta method [13]. This numerical algorithm has been used extensively for simulations compressible turbulent mixing problems, including single shock and reshocked RMI [17, 14, 15].

The initial condition used for all simulations here comes from a recent study of the late-time behaviour of the Richtmyer–Meshkov instability by eight independent LES algorithms [15]. The DNS results are for the standard problem from this study where the initial condition consists of a material interface separating two fluids containing a narrowband perturbation with length scales ranging from $L/8$ to $L/4$ ($L$ is the cross section of the domain). The interface has an initial thickness given by an error function profile with a characteristic width of $L/32$. The initial modes are specified so as to have a constant power spectrum with an overall amplitude of $0.1\lambda_{\text{min}}$. Two sets of ILES results are presented here, one for this same initial condition and the second for an initial condition where the initial length scales are a quarter of the size of those in the standard problem, allowing the simulation to be run to much later non-dimensional time with improved statistical fidelity. The mode amplitudes and phases are defined by deterministic random numbers that are constant for all grid resolutions considered, allowing for a grid refinement study to be performed. Further details on the derivation of the initial perturbation can be found in Thornber *et al.* [17].

The computational domain is Cartesian, with dimensions $x \times y \times z = 2.8\pi \times 2\pi \times 2\pi$ m$^3$ and periodic boundary conditions are used in the $y$ and $z$ directions, with outflow boundary conditions used in the $x$ direction. The initial mean positions of the shock and the interface are $x = 3.0$ m and $x = 3.5$ m respectively and the initial pressure of both fluids is 100 kPa. The evolution of the interface is solved in the post-shock frame of reference ($\Delta u = -291.575$ m/s) and the shock Mach number is 1.8439, equivalent to a four-fold pressure increase. The initial densities of the two fluids are 3 and 1 kg/m$^3$ respectively and the post-shock densities are 5.22 and 1.8 kg/m$^3$. Table 1 gives the thermodynamic properties for both the heavy and light fluids, which are constant throughout the entire domain.

| Property | Heavy Fluid | Light Fluid |
|---|---|---|
| Molecular weight ($W_i$) | 90 g/mol | 30 g/mol |
| Ratio of specific heats ($\gamma_i$) | 5/3 | 5/3 |
| Dynamic viscosity ($\mu_i$) | 0.1 kg/m/s | 0.1 kg/m/s |
| Prandtl No. ($\text{Pr}_i$) | 1.0 | 1.0 |
| Schmidt No. ($\text{Sc}_i$) | 1.0 | 1.0 |

Table 1: Constant thermodynamic properties of the heavy and light fluids. Note: $\mu$, Pr and Sc are for the DNS only.

Four different measures are used to quantify the anisotropy of the mixing layer as it evolves in time. The first is the ratio of components of Favre-avergaed turbulent kinetic energy, which is given by:

$$\text{TKE}(t) = \text{TKX} + \text{TKY} + \text{TKZ} = \int \frac{1}{2}\rho u_i'' u_i'' \mathrm{d}V \qquad (1)$$

where $u_i'' = u_i - \widetilde{u_i}$ and $\widetilde{u_i} = \overline{\rho u_i}/\overline{\rho}$ is a Favre average. A plane average taken over the homogeneous directions is used to calculate the ensemble average $\bar{\phi}$ of a quantity $\phi$. The ratio is then given by:

$$\text{TKR} = \frac{2 \times \text{TKX}}{\text{TKY} + \text{TKZ}} \qquad (2)$$

where a value of $\text{TKR} = 1$ corresponds to complete isotropy of the turbulent kinetic energy components. The second measure used is similar to the first but with components of enstrophy used in place of components of TKE. The enstrophy is defined as:

$$\Omega(t) = \Omega_x + \Omega_y + \Omega_z = \int \rho\omega_i\omega_i \mathrm{d}V \qquad (3)$$

where $\omega_i$ is the vorticity. As with the first measure, a value of $2 \times \Omega_x/(\Omega_y + \Omega_z) = 1$ corresponds to complete isotropy of the enstrophy components. The third measure is a variable-density variant of Lumley's anisotropy tensor, defined by:

$$\mathbf{b}_{ij} = \frac{\langle \rho u_i'' u_j'' \rangle}{\langle \rho u_k'' u_k'' \rangle} - \frac{1}{3}\delta_{ij} \qquad (4)$$

where $\langle \dots \rangle$ indicates a plane average. The diagonal elements of the tensor are bounded between $-1/3$ and $2/3$, with $\mathbf{b}_{ii} = -1/3$ corresponding to no turbulent kinetic energy in the $i^{\text{th}}$ direction and $\mathbf{b}_{ii} = 2/3$ corresponding to all of the turbulent kinetic energy in that direction, while a value of 0 indicates isotropy. Given that the tensor is calculated for each $y-z$ plane, the results presented here are averaged over all $y-z$ planes that satisfy the following condition:

$$4\langle Y_1 \rangle \langle Y_2 \rangle \geq 0.9 \qquad (5)$$

where $Y_i$ is the mass fraction of fluid $i$. Planes that satisfy Equation 5 are referred to as the inner mixing zone [19]. The last measure considered here is the ratio of directional Taylor-scale Reynolds numbers, defined by:

$$\text{Re}_{\lambda_i} = \frac{\langle u_i''^2 \rangle}{\langle \nu \rangle \sqrt{\langle \left(\frac{\partial u_i''}{\partial x_i}\right)^2 \rangle}} \qquad (6)$$

Defining the transverse Taylor-scale Reynolds number as $\text{Re}_{\lambda_{yz}} = (\text{Re}_{\lambda_y} + \text{Re}_{\lambda_z})/2$, the ratio of interest is given by

$\mathrm{Re}_{\lambda_x}/\mathrm{Re}_{\lambda_{yz}}$ where a value of 1 corresponds to isotropy. As with the anisotropy tensor, the results presented here are for $\mathrm{Re}_{\lambda_x}/\mathrm{Re}_{\lambda_{yz}}$ averaged over the inner mixing zone.

### Results

The evolution of the ratio of TKE components in non-dimensional time (defined as $\tau = t\dot{W}_0/\bar{\lambda}$, see [15] for further details) is shown in Figure 1. In the standard case, after an initial peak due to the compression by the shock there is a second peak in both the DNS and ILES data at time $\tau = 0.1845$, with values of 5.113 and 4.573 respectively. Beyond this peak there is a rapid decrease in anisotropy that flattens out into a slow decay, with the DNS data appearing to be converging to the ILES. At the latest point in time the values of this anisotropy measure are 1.701 and 1.423 for the DNS and ILES respectively, with the ILES data seemingly approaching an asymptotic value. However, by examining the behaviour at much later non-dimensional time using the quarter-scale ILES data, it can be observed that the results for the standard case are still in some initial transient stage and are not approaching a steady state. For times later than $\tau \approx 40$ there is a slow but steady decay in anisotropy of TKE components, and although at the latest time there is still 33.6% more fluctuating energy in the $x$-direction this value is still decreasing, presumably asymptotically approaching isotropy.

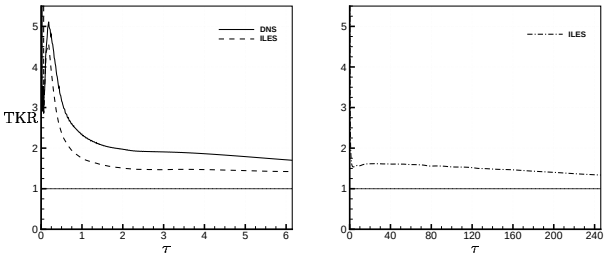


Figure 1: Ratio of turbulent kinetic energy components. Left: Standard case. Right: Quarter-scale case.

In a similar vein as Figure 1, Figure 2 shows the evolution of the ratio of enstrophy components with non-dimensional time. During the initial compression of the layer this ratio is close to 0 as the majority of the vorticity that is deposited baroclinically is confined about the transverse directions (i.e. rotation normal to the plane). The reason for the sharp jump in this ratio at time $\tau = 0.2091$ is due to the shock exiting the domain, at which point there is a large drop in $\Omega_y$ and $\Omega_z$. Interestingly in the standard case the ratio of enstrophy components peaks at a value greater than 1 before declining, this occurs at time $\tau = 0.8365$ for the DNS and time $\tau = 0.5535$ for the ILES. The behaviour after this point is also qualitatively different, with the ILES data asymptoting towards a value of 1 whereas the DNS data is continuing to decrease below 1 at the latest time considered. This is due to the $x$-direction component of enstrophy having a greater decay rate than the transverse components at late times in the DNS. For the later non-dimensional times simulated in the quarter-scale ILES, the ratio of enstrophy components is steadily approaching 1 (the final value is 0.9870), indicating an eventual return to isotropy.

Figure 3 shows the diagonal elements of the anisotropy tensor while Figure 4 shows the ratio of Taylor-scale Reynolds numbers, both averaged across the inner mixing zone, as they evolve in time (note DNS data is the solid line and ILES data is the dashed line). The trends observed here are almost identical to those observed for the ratio of TKE components; after the high anisotropy at compression there is a steady decrease in anisotropy towards what appears to be a steady-state, with the

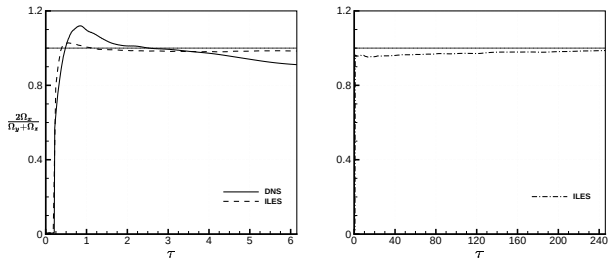


Figure 2: Ratio of enstrophy components. Left: Standard case. Right: Quarter-scale case.

DNS data close to converging to the ILES data at the end of the standard case. The results of the quarter-scale case show that there is an continual return towards isotropy that occurs over a very long period of time. It is useful to compare the values of these two measures with the values for the ratio in TKE components, as this will bring greater insight to the results of previous papers where only presented a single measure has been presented. For the latest time considered in the quarter-scale case the ratio of TKE components is 1.336, which corresponds to a ratio of Taylor-scale Reynolds numbers of 1.281 and values of 0.0536, -0.0287 and -0.0249 for the respective diagonal components of the anisotropy tensor.

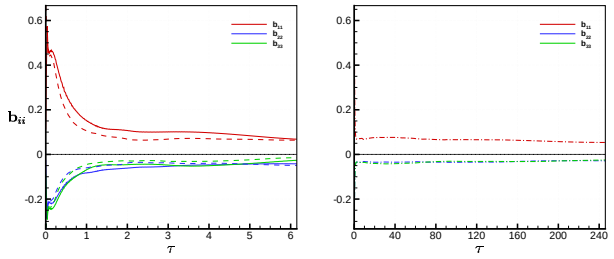


Figure 3: Diagonal elements of the anisotropy tensor. Left: Standard case. Right: Quarter-scale case.

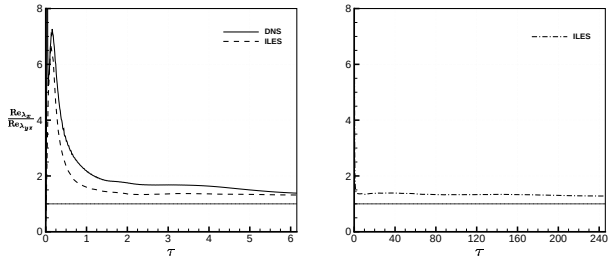


Figure 4: Ratio of Taylor-scale Reynolds numbers. Left: Standard case. Right: Quarter-scale case.

### Conclusions

Anisotropy in the narrowband RMI has been examined by comparing four different measures of anisotropy for three separate simulation databases, an ILES and a DNS of the same nominal case as well as an ILES of a quarter-scale version of the same case to evaluate the behaviour at much later non-dimensional time. The results show that anisotropy is moderately increased at low Reynolds number initially, prior to an apparent return to the high Reynolds number limit at later times. At very late time there is a definite trend towards isotropy although this is not achieved within the period of time considered in the simulation,

indicating that the narrowband RMI is persistently anisotropic over a very large time scale. These results may have important ramifications for models of these flows that assume isotropy over a time scale on the same order as that considered here.


#### Acknowledgements

The authors would like to acknowledge the computational resources at the National Computational Infrastructure through the National Computational Merit Allocation Scheme, as well as the Sydney Informatics Hub and the University of Sydney's high performance computing cluster Artemis, which were employed for all cases presented here.


#### References


[1] Balasubramanian, S., Orlicz, G. C., Prestridge, K. P. and Balakumar, B. J., Experimental study of initial condition dependence on Richtmyer-Meshkov instability in the presence of reshock, *Physics of Fluids*, **24**, 2012, 034103.

[2] Burrows, A., Supernova explosions in the Universe, *Nature*, **403**, 2000, 723–733.

[3] Clark, D. S., Weber, C. R., Eder, D. C., Haan, S. W., Hammel, B. A., Hinkel, D. E., Jones, O. S., Kritcher, A. L., Marinak, M. M., Milovich, J. L., Patel, P. K., Robey, H. F., Salmonson, J. D., Sepke, S. M. and Edwards, M. J., Three-dimensional simulations of low foot and high foot implosion experiments on the National Ignition Facility, *Physics of Plasmas*, **23**.

[4] Grinstein, F. F., Gowardhan, A. A. and Wachtor, A. J., Simulations of Richtmyer-Meshkov instabilities in planar shock-tube experiments, *Physics of Fluids*, **23**, 2011, 034106.

[5] Kim, K. H. and Kim, C., Accurate, efficient and monotonic numerical methods for multi-dimensional compressible flows Part II: Multi-dimensional limiting process, *J. Comput. Phys.*, **208**, 2005, 570–615.

[6] Livescu, D., Numerical simulations of two-fluid turbulent mixing at large density ratios and applications to the Rayleigh-Taylor instability, *Philosophical Transactions of the Royal Society of London A: Mathematical, Physical and Engineering Sciences*, **371**, 2013, 20120185.

[7] Lombardini, M., Pullin, D. I. and Meiron, D. I., Transition to turbulence in shock-driven mixing: A Mach number study, *Journal of Fluid Mechanics*, **690**, 2012, 203–226.

[8] Meshkov, E. E., Instability of the interface of two gases accelerated by a shock wave, *Fluid Dyn.*, **43**, 1969, 101–104.

[9] Mohaghar, M., Carter, J., Musci, B., Reilly, D., McFarland, J. and Ranjan, D., Evaluation of turbulent mixing transition in a shock-driven variable-density flow, *Journal of Fluid Mechanics*, **831**, 2017, 779–825.

[10] Oggian, T., Drikakis, D., Youngs, D. L. and Williams, R. J., Computing multi-mode shock-induced compressible turbulent mixing at late times, *Journal of Fluid Mechanics*, **779**, 2015, 411–431.

[11] Reese, D. T., Ames, A. M., Noble, C. D., Oakley, J. G., Rothamer, D. A. and Bonazza, R., Simultaneous direct measurements of concentration and velocity in the Richtmyer-Meshkov instability, *Journal of Fluid Mechanics*, **849**, 2018, 541–575.

[12] Richtmyer, R. D., Taylor Instabilities in Shock Acceleration of Compressible Fluids, *Communications on Pure and Applied Mathematics*.

[13] Spiteri, R. J. and Ruuth, S. J., A class of optimal high-order strong-stability preserving time discretization methods, *SIAM J. Num. Anal.*, **40**, 2002, 469–491.

[14] Thornber, B., Impact of domain size and statistical errors in simulations of homogeneous decaying turbulence and the Richtmyer-Meshkov instability, *Physics of Fluids*, **28**.

[15] Thornber, B., Griffond, J., Poujade, O., Attal, N., Varshochi, H., Bigdelou, P., Ramaprabhu, P., Olson, B., Greenough, J., Zhou, Y., Schilling, O., Garside, K. A., Williams, R. J., Batha, C. A., Kuchugov, P. A., Ladonkina, M. E., Tishkin, V. F., Zmitrenko, N. V., Rozanov, V. B. and Youngs, D. L., Late-time growth rate, mixing, and anisotropy in the multimode narrowband Richtmyer-Meshkov instability: The θ-group collaboration, *Physics of Fluids*, **29**.

[16] Thornber, B., Mosedale, A., Drikakis, D., Youngs, D. and Williams, R., An Improved Reconstruction Method for Compressible Flows with Low Mach Number Features, *J. Comput. Phys.*, **227**, 2008, 4873–4894.

[17] Thornber, B., Youngs, D., Drikakis, D. and Williams, R. J. R., The influence of initial conditions on turbulent mixing due to Richtmyer-Meshkov Instability, *J. Fluid Mech.*, **654**, 2010, 99–139.

[18] Toro, E. F., Spruce, M. and Speares, W., Restoration of the contact surface in the HLL-Riemann solver, *Shock Waves*, **4, 1**, 1994, 25–34.

[19] Tritschler, V. K., Olson, B. J., Lele, S. K., Hickel, S., Hu, X. Y. and Adams, N. A., On the Richtmyer–Meshkov instability evolving from a deterministic multimode planar interface, *Journal of Fluid Mechanics*, **755**, 2014, 429–462.

[20] Tritschler, V. K., Zubel, M., Hickel, S. and Adams, N. A., Evolution of length scales and statistics of Richtmyer-Meshkov instability from direct numerical simulations, *Phys. Rev. E*, **90**, 2014, 63001.

[21] Weber, C. R., Clark, D. S., Cook, A. W., Busby, L. E. and Robey, H. F., Inhibition of turbulence in inertial-confinement-fusion hot spots by viscous dissipation, *Physical Review E*, **89**.

[22] Yang J., K. T. and Zukoski, E., Applications of shock-induced mixing to supersonic combustion, *AIAA Journal*, **31**, 1993, 854–862.

[23] Youngs, D. L., Numerical simulation of mixing by Rayleigh-Taylor and Richtmyer-Meshkov instabilities, *Laser Part. Beams*, **12**, 1994, 725–750.

[24] Zhou, Y., Rayleigh-Taylor and Richtmyer-Meshkov instability induced flow, turbulence, and mixing. I, *Physics Reports*, **720-722**, 2017, 1–136.

[25] Zhou, Y., Rayleigh-Taylor and Richtmyer-Meshkov instability induced flow, turbulence, and mixing. II, *Physics Reports*, **723-725**, 2017, 1–160.